Annual Report

DOE DE-FG52-06NA26213

3/1/07-2/29/08

PI: Nigel D. Browning
Department of Chemical Engineering and Materials Science
University of California-Davis
Davis, Ca 95616

Co-PI: W. Andreas Schroeder
Department of Physics
University of Illinois-Chicago
Chicago, IL 60607

Co-PI: John C. H. Spence
Department of Physics
Arizona State University
Tempe, AZ 85287

Statement of Work for Year 2

The work performed in this project is aimed at developing routine methods for the operation of an optimized DTEM to study strongly driven materials, aging and corrosion and nanoscale materials. There are three main aspects of this work. The first aspect concerns the performance of advanced measurements on several materials systems using the DTEM at Lawrence Livermore National Laboratory (this aspect of the project is being performed at UC-Davis). The aim of the second year of work at UC-Davis was to develop the techniques for coherent diffractive imaging (CDI) in the DTEM. In addition, the plan was to perform initial experiments using the in-situ stage. The second aspect of this project that is being performed at UIC is aimed at improving the temporal and spatial resolution of the microscope. The plan for year 1 included the construction of a versatile ultrafast electron microscope (UEM) test column, and interface the column with both the available, state-of-the-art, diode-pumped, ultrashort-pulse laser system and parts from a decommissioned JEM 100CX electron microscope (the magnetic electron lens, scintillator, and sample holder stage). The third aspect of this project that is being performed at ASU, aims to test the viability of a pulsed photo-field-emission source. The plan for year 1 of this research focused the construction of a test chamber for the emitter.

1. A narrative discussion of accomplishments

Work performed at UC-Davis has attempted to identify the limitations in temporal and spatial resolution in the DTEM and design experimental procedures to improve them. In order to directly image structural changes taking place in metallic and semiconducting nanostructures in the DTEM it is desirable to overcome spatial and temporal limitations induced by Coulombic effects as an electron pulse travels through the microscope column. These effects become particularly detrimental to image resolution at crossover points present when the electron lenses are set to imaging mode. One approach to solving this problem is to collect data in diffraction mode (where the crossovers are much less compact) and reconstruct images from the recorded diffraction patterns using iterative phase retrieval algorithms. This method known as Coherent Diffractive Imaging (CDI) utilizes an iterative cycle in which constraints placed on the data in both reciprocal and real space allow for a unique solution of the lost phase information.

Thus far the CDI work done for this project has been performed using the familiar Hybrid Input Output algorithm. The tendency of this algorithm to stagnate in local minima in hyper-dimensional search spaces is a well documented problem. Recent algorithm development work has focused on incorporating global search algorithms with HIO to help avoid these stagnation issues. Initial attempts involved the use of genetic algorithms with little success; however recent attempts to incorporate Particle Swarm Optimization (PSO) have led to some promising results. PSO algorithms are a class of global search algorithms that seek out global minima by emulating social behavior such as bird flocking or fish schooling. The combination of these two techniques, tentatively called Swarm Optimized Phase Retrieval (SOPR), initializes the “particles” by assigning a random set of phases for the known modulus of the diffraction pattern. Each particle is then run through a series of iterative phase retrieval algorithms, specifically the Hybrid

Input Output (HIO) algorithm and the Error Reduction (ER) algorithm. The error metrics for these algorithms can then be used to choose a personal best solution for each particle and global best solution from all of the particles. These solutions drive a velocity equation that shifts the position of each particle in the search space. As shown by equation 1, this velocity update equation drives particles out of the search paths defined by HIO towards the global and personal best solutions, thereby allowing individual particles to escape local minima (the r coefficients are randomized at every iteration). This final step allows particles to escape local minima in the search space and thereby avoid the stagnation problems common to HIO and ER (a schematic of the operation is shown in figure 1)

$$V_{n+1} = c_1 V_n + c_2 r_1 \circ (P_B - P_n) + c_3 r_2 \circ (G_B - P_n)$$

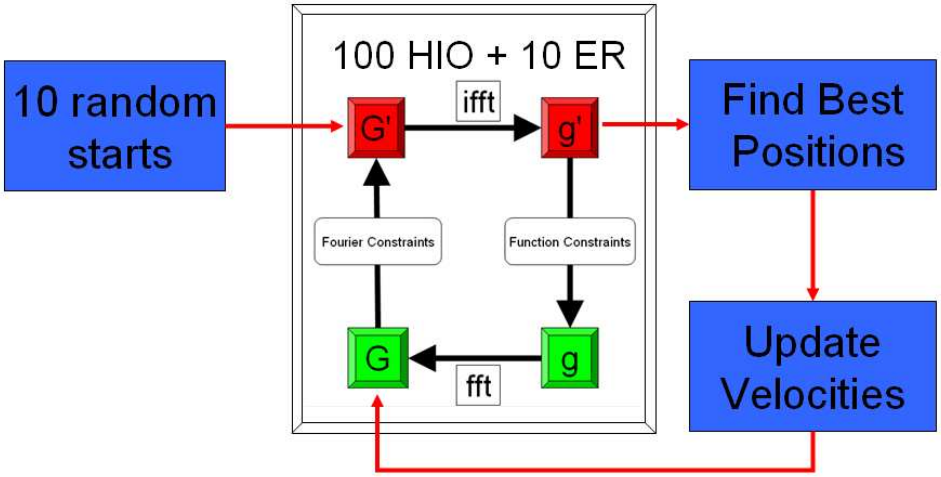

Figure 1. Flowchart of the steps involved in the SOPR algorithm including the generic cycle for iterative phase retrieval algorithms which are at the core of SOPR

The most promising initial results have been obtained using simulated data with a circular support, a problem that is notoriously difficult for the standard iterative phase retrieval algorithms. As the symmetry of the support area is increased the likelihood of stagnation in local minima drastically increases. Thus CDI of a circular support region, a case that is likely to arise in DTEM studies of catalyst nanoparticles, is particularly likely to suffer from stagnation in local minima. The images reconstructed from these stagnated solutions are characterized by low resolution sinusoidal striations covering low intensity areas. Figure 1 shows a comparison of the performance of SOPR vs. HIO on simulated data with a circular support. While these results are promising, a significant amount of analysis is still required to determine how robust SOPR is compared to HIO/ER. All global search algorithms (and particularly ones such as SOPR with a complicated parameter space), are all subject to a problem known as “no free lunch”. This essentially means that a given parameter set will not be optimal for every problem. Since SOPR involves over 10 parameters a huge amount of analysis will have to be done on both simulated and experimental data before it can be conclusively stated that SOPR outperforms HIO.

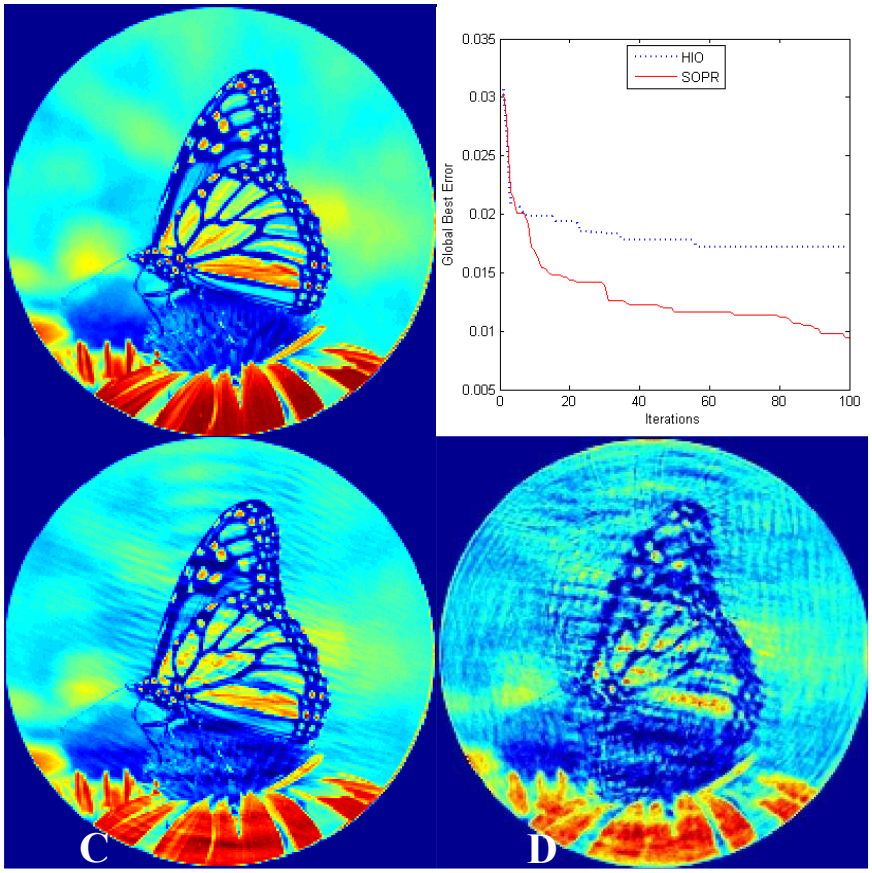

Figure 2. Comparison of SOPR and HIO performance on a highly symmetric support. A. Original image. B. Graph of the object domain error metric for HIO and SOPR algorithms run over 100 iterations. C. Global best result from SOPR using 10 particles. D. Best result from HIO out of 10 random starting phases.

In addition to the work performed on the development of CDI for the DTEM, an in-situ stage has also been developed. This stage is being purchased with funds separate from this project (supplied by ExxonMobil corporation), but will play a key role in the ability to observe materials properties under dynamic conditions. The commissioning of the environmental holder from Fischione Instruments is now nearly complete. In initial tests on the JEOL 200CX at LLNL (comparable in resolution and properties to the DTEM) the holder showed strong promise for fast exchange and viewing of nanostructure evolution. Specifically, pump down time for the holder was comparable to traditional TEM holders. Resolution was limited by the SiN windows, however we were able to resolve nanowires and nanoparticles less clearly to ~1nm in BF and STEM modes. Compared to the prototype, a change in the overall design was implemented, and the holder incorporated new seals to prevent leakage, and changed the sample placement to the 'bottom' window to improve resolution. The holder experienced zero leakage, and much improved resolution with the new window configuration. Additionally, we found that there was minimal drift during gas flow. Figure 3 shows AuMgO particle aggregation on a lacey carbon grid during flow of 5% H_2 in N_2 at room temperature. The images indicate time and flow rate, which was controlled with mass flow controllers (run

in a labview interface). Figure 4 shows more AuMgO nanoparticles on lacey carbon. In this case, we started the sample at a high flow rate of % H_2 in N_2 at room temperature, and held it at this rate for 9 minutes, then closed the valve completely, switching to a 0 flow rate. Though there was some drift, we could still view the particles without moving the sample at all. The results are extremely promising for environmental in situ experiments in the DTEM. Final configuration changes to the holder are currently being implemented with the holder expected to be in place at Davis in April 2008.

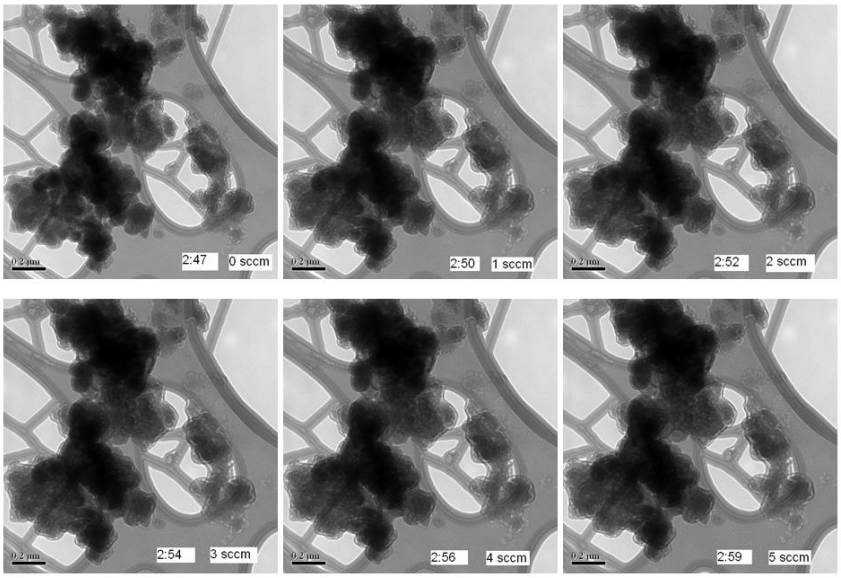

Figure 3. Images obtained in tests of the in-situ stage during flow rates of a H_2/N_2 gas mix of 0 to 5 SCCM at room temperature.

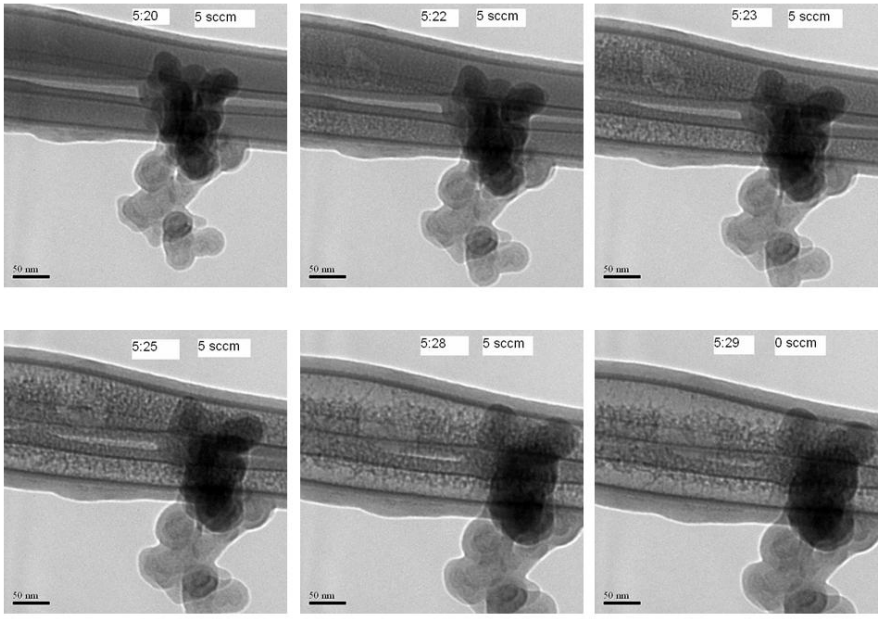

Figure 4. Images of AuMgO aggregation in 5 SCCM H_2/N_2 at room temperature.

The accomplishments in Year 2 of the UIC portion of the three-year research project can be separated into five categories:

- Stationing of the electron gun and DTEM development project into dedicate laboratory facilities.
- Development, characterization, and installation of a new femtosecond drive laser for the DTEM – a diode-pumped, thermal lens shaped (TLS), soliton mode-locked (ML) Yb:KGW laser.
- Re-design of the DC photoelectron gun for improved performance in an ultrafast electron microscope (UEM).
- Acquisition and testing of hexaboride crystals (low work function) and plane holographic gold gratings (plasmon-enhanced photoemission) to find high-performance and low emittance photocathodes.
- Determination of the appropriate RF cavity design for electron pulse compression in the UEM.

This work has solved and will solve some of the problems encountered in the development of a functional prototype UEM test column employing available parts from a decommissioned JEM 100CX electron microscope (the magnetic electron lens, scintillator, and sample holder stage) and interfaced with a high-power, ultrashort-pulse laser system.

Dedicated UEM laboratory

In September 2007, the research project was moved into a dedicated ultrafast electron microscopy laboratory in the Research Resources Center – East (RRC-East) of the University of Illinois at Chicago (UIC), which also houses a number of other electron microscopes associated with the Electron Microscopy Services (EMS) of UIC. The dedicated laboratory space was selected to ensure that a suitable environment for the UEM. Specifically, the laboratory has low intrinsic floor vibrations (below 10 microns/s/√Hz) above ~100Hz and its walls are already fitted with panels of acoustic foam damping. To further reduce the influence of vibrations, the custom U-shaped optical table acquired to couple the microscope column to the laser radiation source is placed on active vibration isolation legs to damp efficiently vibrations below 100Hz. Together with the air-conditioning (e.g., temperature) control, this laboratory provides a very suitable environment for the development of a high time-space resolution UEM.

Figure 5 depicts the dedicated UEM laboratory with the frequency-doubled (green light) laser system in the background and the 10-50kV electron gun in the foreground. The custom 4x7 ft. U-shaped and vibration isolated optical table is designed to hold the projected ~1000 lbs microscope column in the 2x2 ft. open center section; our laser-driven electron gun on top of the bottom imaging section of a JEM 100CX column from decommissioned microscope.

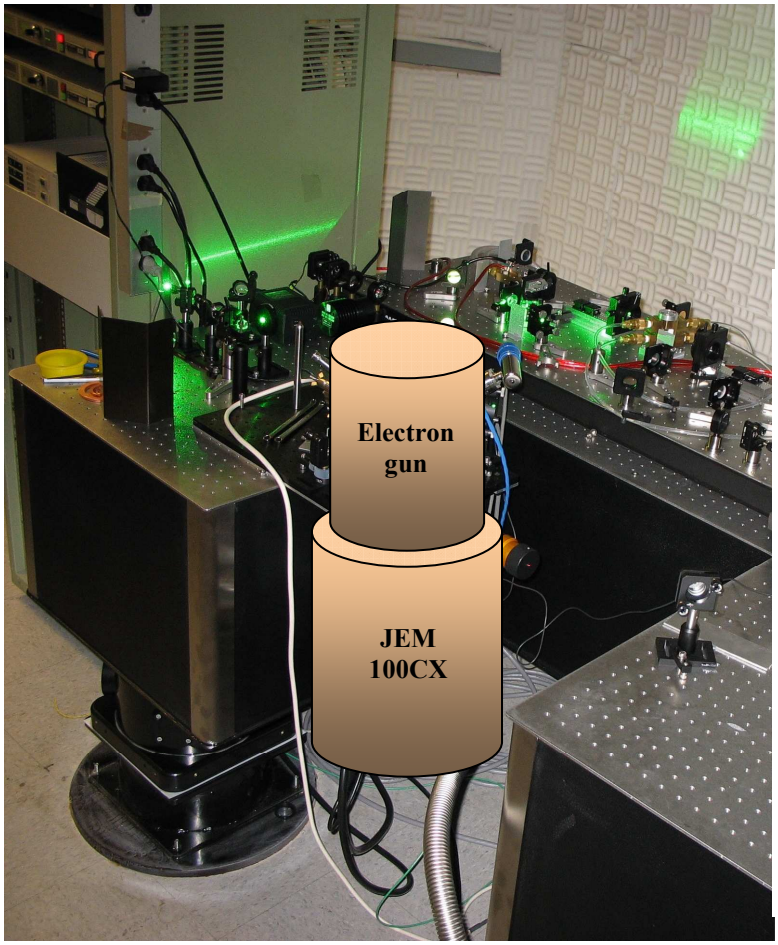

Figure 5. The dedicated UEM laboratory in RRC-East with the U-shaped optical table and frequency-doubled femtosecond Yb:KGW laser system (back right). The future position of the ultrashort pulse electron gun on top of the JEM 100CX electron microscope column is also shown.

Femtosecond drive laser for photo-electron gun

The first year's experimental and theoretical work on the development of a laser-driven ultrashort pulse electron gun for a DTEM clearly showed that the initial electron pulse shape strongly dictates the subsequent space-charge induced space-time pulse dynamics upon propagation down the microscope column. In particular, as shown in Figure 6, an electron pulse with an initial spatial diameter ($2w$) much greater than its longitudinal length ($v\tau$, where v and τ are the pulse velocity and temporal duration, respectively) mainly suffers space-charge induced temporal pulse broadening. Conversely, a pulse with initially $v\tau >> 2w$ will predominantly broaden in the transverse spatial direction. In other words, the shortest initial electron pulse dimension undergoes the largest space-charge induced acceleration due to the fact that the internal space-charge field is greatest in this direction. Accordingly, if one intends to study and optimize the spatial electron emission characteristics of a laser-driven photo-electron gun, an operational regime that segregates the space-charge effects into the longitudinal propagation direction is clearly strongly preferred; that is, one requires $v\tau << 2w$ in order for the space-charge effects not to interfere with the optimization of the spatial emittance of an ultrafast electron gun. Moreover, as discussed below, the consequent longitudinal temporal pulse broadening can be compensated and corrected for through the use of a suitably phased RF accelerator cavity.

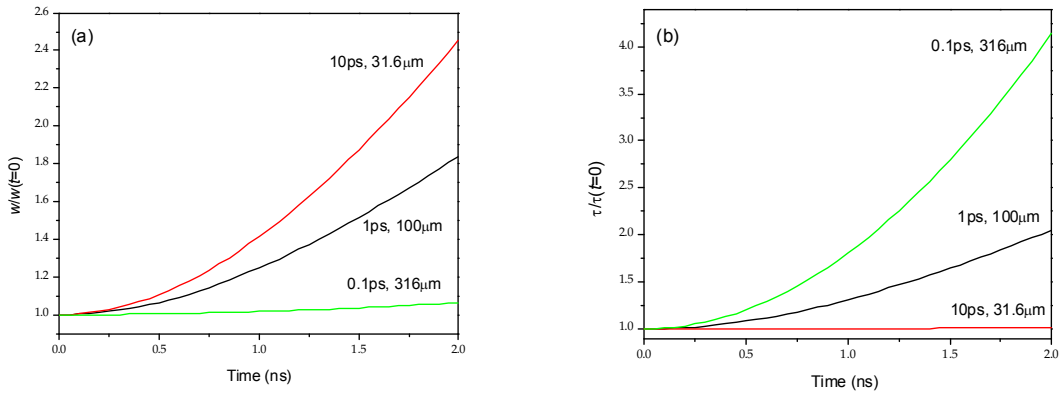

Figure 6. Space-time dynamics of Gaussian, radially-symmetric, 5,000-electron pulses with durations of 0.1ps (green), 1.0ps (black), and 10ps (red) and the same initial peak charge density: (a) normalized transverse beam waist w and (b) normalized pulse duration τ as a function of propagation time.

The above argument, coupled with the requirement to reduce overall space-charge effects by reducing the pulse charge density, implies that the largest possible electron pulse diameter ($2w$) should be used in a UEM. However, unlike beams for high-energy physics particle accelerators, for a functional UEM one is restricted generally to electron beam diameters of ~1mm – the maximum acceptance aperture of modern electron optics (i.e., magnetic lenses). As a result, for typical electron velocities $v \approx c/2$ (c is the speed of light), the required condition that $v\tau << 2w$ means that the electron pulse duration τ, and hence the incident laser pulse duration generating the electron pulse, should be less than about 1ps. This realization has led us to replace the previously employed 60MHz, 8W, mode-locked Nd:$GdVO_4$ laser producing ~10ps pulses at 1063nm [1] with a laser radiation source generating pulses with sub-picosecond durations. A schematic of this latter home-built, diode-pumped, high-power, femtosecond Yb:KGW (Yb-doped potassium gadolinium tungstate) laser resonator [2,3] is shown in Figure 7. As with the Nd:$GdVO_4$ laser, the successful thermal lens shaping (TLS) technique [4] is employed in the pumping of the Yb:KGW gain medium to ensure an astigmatism-compensated optical cavity for fundamental TEM_{00}-mode operation.

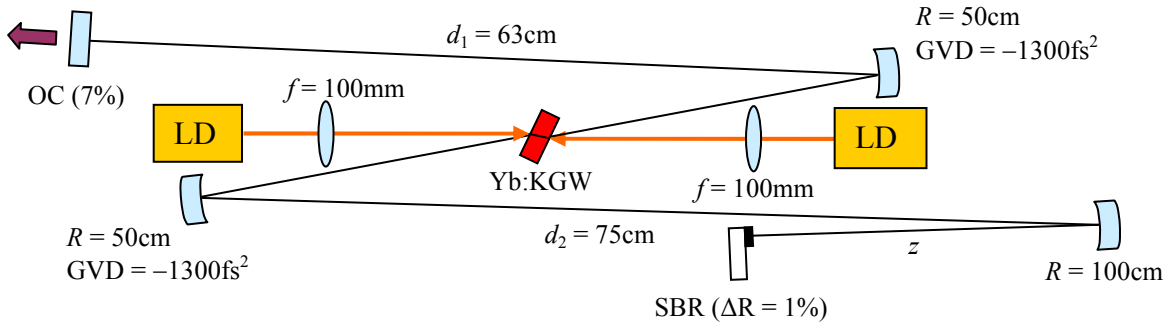

Figure 7. Schematic of the femtosecond TLS Yb:KGW oscillator (LD = laser diode, OC = output coupler, SBR = saturable Bragg reflector).

In the configuration shown in Figure 7 with $z \approx 42$cm and a net round-trip negative group velocity dispersion (GVD) of -5200fs^2 introduced by the two 50cm radius of curvature z-fold mirrors, the Yb:KGW laser exhibited self-starting soliton mode-locking for output powers above ~2W. The maximum (or optimum) mode-locked output power obtained without the emergence of DC spectral components was 3.5W, with a sech^2 pulse duration of 250fs (Fig. 8(a)). The insertion of two further plane dispersion compensation mirrors each with a GVD of -700fs^2 into the short arm of the cavity generated higher mode-locked output powers with longer pulse durations. For example, with two reflections off each mirror (an additional -5600fs^2 of round-trip GVD), the pulse duration increased to 347fs (Fig. 8(b)) at an optimum mode-locked output power of 5.0W. This trend is consistent with the expected 'soliton' mode-locking regime; that is, the SBR only initiates the mode-locking mechanism, which is quickly dominated by self-phase modulation in the Yb:KGW gain medium balanced by the net negative GVD in the cavity [5].

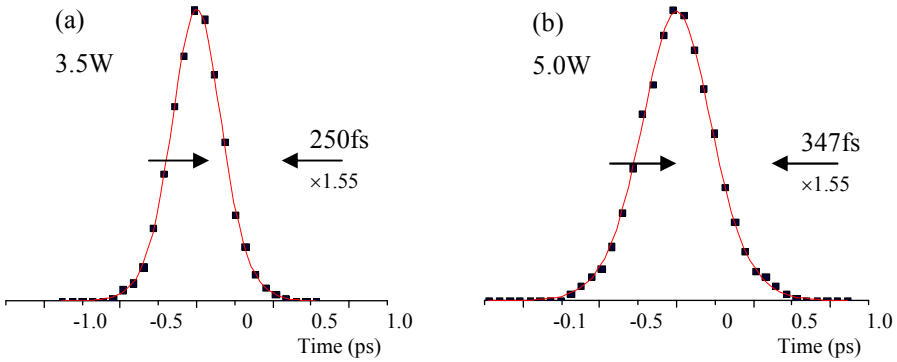

Figure 8. Second harmonic autocorrelation measurements of the laser pulse duration and fits assuming a sech^2 pulse shape; (a) for the cavity depicted in Fig. 3 and (b) with an additional -5600fs^2 of round-trip GVD

The data shown in Figure 9 illustrates the performance characteristics of the femtosecond TLS Yb:KGW laser in the resonator configuration of Figure 7. A clear ~250mW increase in the fundamental output power at 1040nm is observed when the laser switches from continuous-wave (CW) to ML operation, indicating an increase in the net quality (or Q) of the cavity oscillation for pulsed operation that is consistent with the stability of the laser under ML operation. Also shown in Figure 9 is the green power at 520nm obtained by frequency doubling the ML laser output in a 2mm-thick, Brewster-cut and critically phase-matched lithium triborate (LBO) crystal. A clear saturation in the doubled green power at 1.65W for diode currents above 30A is consistent with the observed emergence of CW spectral components in the fundamental output in this regime; that is, for operation above the 'soliton power limit' of the laser. Frequency doubling efficiencies in excess of 60% are observed for our z-fold doubling geometry, which employs a crystal length of the same order as the confocal parameter of the

focused fundamental wave and is optimized to minimize the effects of group velocity mismatch and spatial beam walk-off.

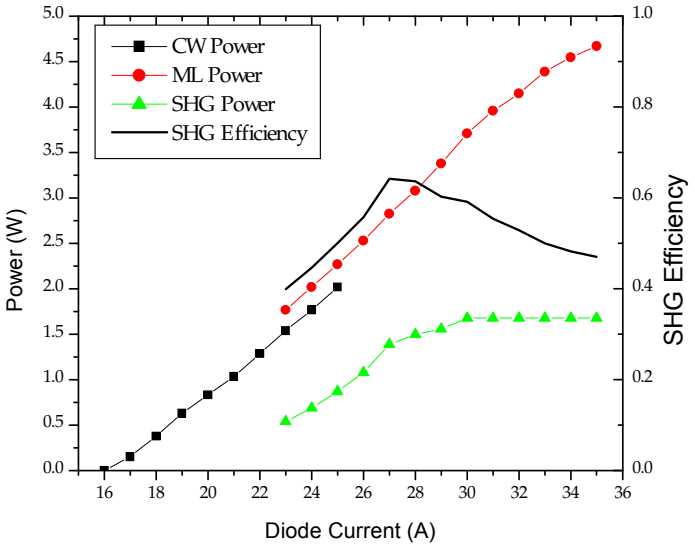

Figure 9. Output power performance of the TLS femtosecond Yb:KGW laser as a function of diode laser current: CW (black squares) and ML (red circles) fundamental output power; second harmonic power (green triangles) and conversion efficiency (line) from a 2mm-thick, Brewster-cut, LBO frequency doubling crystal.

The sub-picosecond green laser pulses generated by frequency doubling the output from the ML Yb:KGW laser are ideally suited for driving the photocathode in our electron gun. Their ~200fs duration clearly fulfills the requirement that $v\tau << 2w$ for an incident laser beam diameter of ~1mm. Moreover, for the ~1W of average power at the laser repetition rate of 63MHz (implying a peak pulse power of 80kW), the oscillating laser field strength on the surface of the photocathode will be ~10MV/m. This is well in excess of the ~10kV/cm DC field strength of our electron gun. Consequently, with a suitable photocathode material, such as a nano-patterned photocathode, it should be possible for the laser field to assert some linear or nonlinear control over the electron photoemission process, thereby decreasing the emittance of our electron gun.

DC photoelectron gun re-design

In the second project year, we have also re-designed the anode and cathode shapes and configurations in our DC photoelectron gun with a view to improving the overall gun performance. The new DC gun design shown in Figure 10 is based on that employed by Togawa et al. [6] in their 500kV, CeB_6 (cerium hexaboride), large-area (3mm diameter) and high-current, thermionic emission gun. The use of both polished and cleaned stainless steel and the curved features on the anode and Wehnelt encapsulating the photocathode allow high DC field strengths to be obtained. In addition, the use of a relatively large anode beam orifice and the specific 1:1 ratio between the radius of the

exit hole in the anode and the radius of its curved surface ensures that the anode is a minimally divergent electrostatic lens (Fig. 10(b)) for our electron beam diameters of ~1mm. The design also allows for incident laser beam angles θ of between 45 and 60 degrees (Fig. 10(a)) and can readily accept photocathode area sizes up to 0.5x0.5 inches.

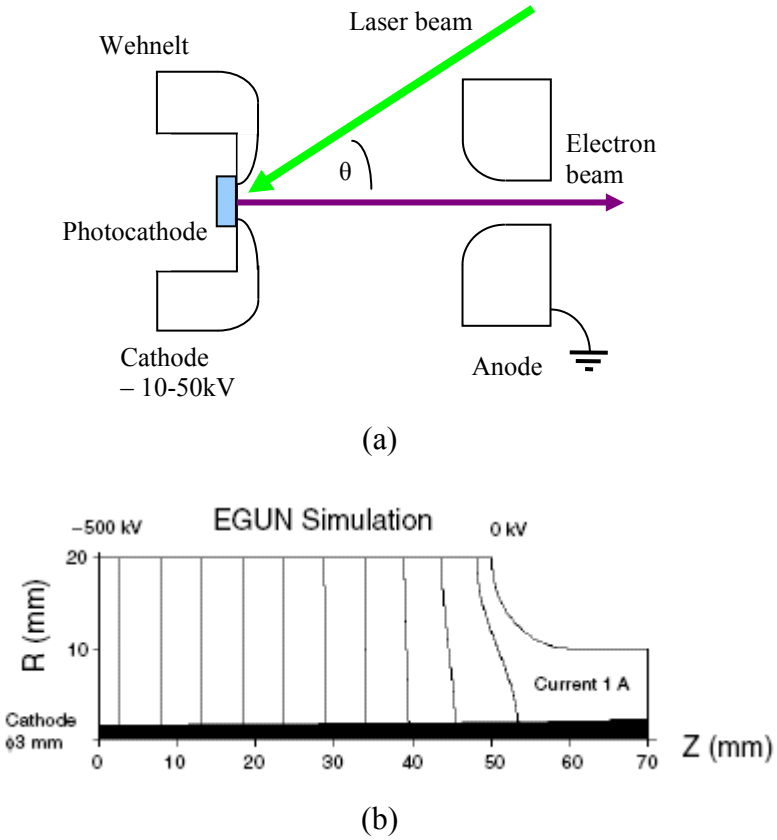

Figure 10. (a) Schematic of the re-designed 10-50kV DC photoelectron gun based on the work of Togawa et al. [6]. (b) Simulation of the equipotentials in the 500kV gun design of Togawa et al. [6] with the 3mm-diameter electron beam (solid black).

Photocathodes: Hexaborides and plane holographic gold gratings

Work is currently underway to study the emission properties of two types of photocathodes using the powerful ~200fs green (520nm) pulses from the frequency doubled, ML Yb:KGW laser: (i) the semi-metallic hexaborides LaB_6 (100) and CeB_6 (310) and (ii) plane holographic (i.e., sinusoidal) gold-coated diffraction gratings with 750 lines/mm. In all cases, cylindrical optics are used to ensure that a circular area is illuminated on the photocathodes (i.e., to compensate for the ~50º angle of incidence) and a YAG scintillation crystal is employed to determine electron beam ellipticity. Additionally, a Faraday cup charge detector equipped with a retardation grid (Kimball Physics model FC-73A) is used to measure both the electron charge per laser pulse and the photoelectron energy spread.

The two hexaborides have work functions Φ of about 2.7 and 2.4eV, respectively. When compared to the 2.39eV photon energy of 520nm radiation, this means that one might only expect minimal single-photon photoemission from the (310)-cut CeB_6 crystal due to the finite bandwidth ($\Delta E \approx 10$meV) of the femtosecond green laser pulses and the

thermal tail ($k_B T$ = 25meV) of the Fermi distribution function at 300K. However, the Schottky effect, the suppression of the work function due to the applied surface field E_s (e.g., the DC gun field), must also be taken into account;

$$\Phi_{eff.} = \Phi - \frac{e}{2}\sqrt{\frac{eE_s}{\pi\varepsilon_0}} \quad , \tag{1}$$

where e is the fundamental electron charge and ε_0 is the vacuum permittivity. For a DC field of 10kV/cm, the effective work function $\Phi_{eff.}$ is 38meV lower than Φ, which already allows single-photon photoemission from CeB_6 (310) with an average electron excess energy of about 20meV. Furthermore, this analysis does not take into account the stronger ~10MV/m laser field amplitude at the surface of the photocathode, which induces an additional oscillating change in the work function of $\Delta\Phi \approx \pm 0.12$eV. This variation is sufficiently large to both 'switch-off' the photoemission process when the laser field is oriented to oppose the applied DC field and to enhance the photoemission efficiency (proportional to the square of the excess energy) in one radiation period (~1.7fs at 520nm). If the photoemission process is indeed instantaneous, this effect will be observable through a change in the photoelectron energy spread as a function of the incident laser power.

For the LaB_6 (100) crystal, the larger 2.7eV work function should prohibit single-photon photoemission even in the presence of the oscillatory Schottky effect. It therefore represents a control experiment. However, two-photon photoemission and photo-assisted field emission [7,8] are possible. If electron emission is observed, these two processes can be distinguished through their significantly different energy spreads. We also note in passing that efficient single-photon photoemission from CeB_6 (310) driven by 520nm femtosecond laser pulses, in the absence of space-charge effects, would produce a very useful pulsed electron source for a UEM since its intrinsic energy spread would be less than 0.1eV.

Plane holographic gold gratings have interesting and anomalous multi-photon photoemission properties under visible or near-infrared irradiation when a surface plasmon resonance with the periodicity of their sinusiodal surface structure is excited. This is because the local dipole field associated with the surface plasmon can be many orders of magnitude stronger than the incident driving laser field. As a result, photoemission properties are greatly perturbed by the collective electronic plasmon oscillation; for example, the oscillatory Schottky barrier suppression (equation (1)) can exceed 1eV. As gold has a work function of 5.1eV, this will allow plasmon-enhanced two-photon photoemission with our femtosecond 520nm (2.39eV) laser pulses.

The condition for first-order resonant excitation of a surface plasmon on a grating with period a is

$$\sin\theta = \sqrt{\frac{\varepsilon}{1+\varepsilon}} - \frac{\lambda}{a} \quad , \tag{2}$$

where θ is the angle of incidence of the laser light of wavelength λ, and ε is the real part of the dielectric function of the grating – the noble metal coating in our case. For a gold grating with 750 lines/mm irradiated at 520nm, the surface plasmon phase-matching condition of equation (2) gives $\theta \approx 50^{\circ}$. In addition, *p*-polarized incident laser radiation is required in order to couple to the surface plasmon oscillation perpendicular to grating surface. Both of these conditions can be achieved with our re-designed laser-driven DC gun. We will also employ well-known optical techniques to tilt the pulse front of the femtosecond laser pulse to 50º to compensate for the large angle of incidence; that is, ensure that the temporal distortion due to propagation of the pulse front across the ~1mm laser beam diameter on the photocathode is not a factor in the initial photo-generated electron pulse duration.

In addition to enhancing the photoemission efficiency, the surface plasmon field also affects the angular distribution of the photoemission. Specifically, the pondermotive force experienced by the emitted electrons in the strong local plasmon field restricts their transverse momentum distribution perpendicular to the grating grooves [9]. This effect, which generates an elliptical spatial electron beam profile (with the major axis parallel to the grating grooves), should be readily observable with a YAG scintillation screen. On the other hand, the longitudinal energy spread of the electrons is also increased by roughly the pondermotive potential energy associated with the oscillating plasmon field [10,11]. This effect can produce energy spreads of the order of 10eV. Fortunately, it may be possible to compensate for the resultant temporal electron pulse distortion and significantly reduce the energy spread of the electron pulse at the specimen using an RF cavity, as discussed below.

The natural extension of the inherently one-dimensional grating is to employ a two-dimensional sinusoidal grating structure – a 'criss-cross' grating with an array nano-emission points. Such optical elements are available commercially and their performance as a photocathode will also be assessed. The idea here, of course, is to reduce the momentum distribution in both transverse dimensions and thereby substantially decrease the emittance of the DC electron gun. The study of a criss-cross grating plasmon-enhanced photoemitter will also serve as a natural precursor to the planned investigations of nano-patterned photocathodes based on periodic arrays of gold nano-disks on a silicon substrate – a component that is currently being manufactured at the Northern California Nanotechnology Center (NC2) at UC-Davis. In addition, we plan to investigate the reported $\sim 10^3$-fold enhancement in photoemission efficiency when a thin 30-50nm-thick gold layer is deposited on a plane sinusoidal holographic Al grating [11]. In this case, the two plasmons at the air-Au and Au-Al interfaces coherently couple to further enhance the plasmon-enhanced photoemission mechanism. Clearly, such a large enhancement in photoelectron generation efficiency will benefit the development of an operational UEM.

Longitudinal space-charge effects and RF cavity pulse compression

The modeling of ultrashort electron pulse propagation initiated in the first year of the project has been extended to describe the electron pulse dynamics from the DC gun to the specimen in the preferred operational limit of a UEM with 'disk-like' pulses (i.e., 2*w*

>> $v\tau$). In this limit, as shown in Figure 1, one may safely neglect the influence of space-charge on the spatial pulse dynamics. In other words, the space-charge field E_{SC} is assumed to be solely axial with a magnitude equal to $\frac{\sigma}{2\varepsilon_0}$, where $\sigma = -\frac{Ne}{\pi w^2}$ is the surface charge density of the electron pulse containing N electrons. This then allows the formulation of a simple non-relativistic model of the electron pulse propagation dynamics down the microscope column.

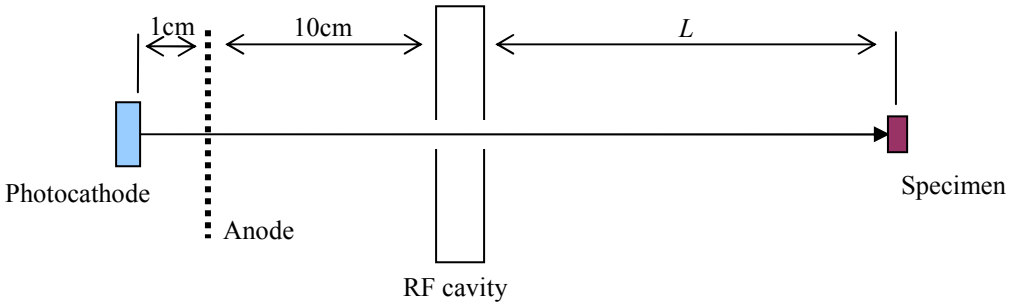

(a)

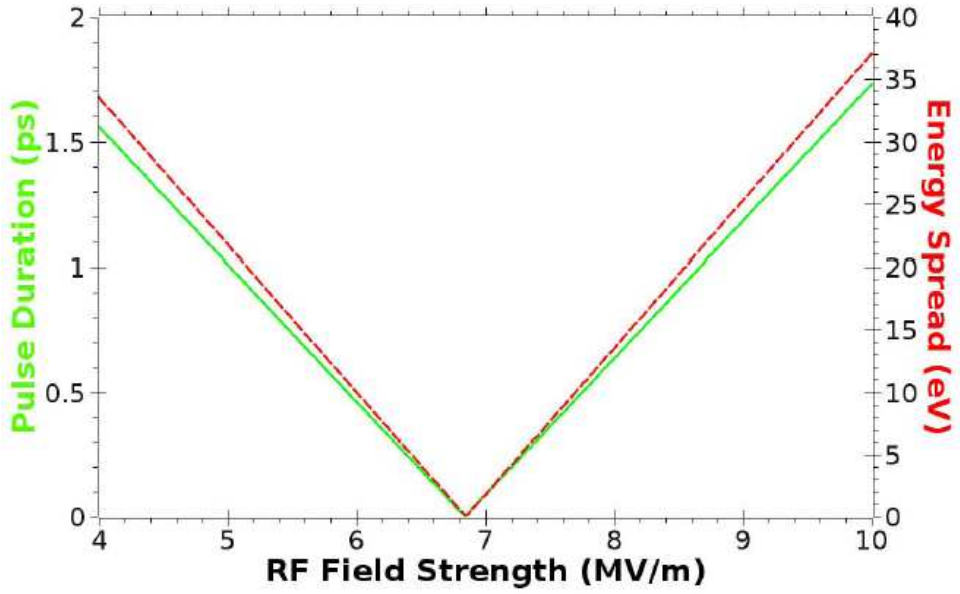

(b)

Figure 11. (a) Schematic of the modeled UEM column; (b) Electron pulse duration (green) and energy spread (red) at the specimen as a function of RF field strength for V_{DC} = 30kV, $\hbar\omega - \Phi$ = 1eV, E_{SC} = 100V/m, ν_{RF} = 1.4GHz, and L = 28.8cm.

The model evaluates the effects of the axial space-charge field and the initial energy spread upon photoemission on the front and back of the electron pulse as it propagates down the canonical UEM column (photocathode to specimen) shown in Figure 11(a). As expected, the model shows that the energy spread due to photoemission,

$\Delta E = \hbar\omega - \Phi = \frac{1}{2} m v_{\max.}^2$ for single-photon photoemission, dominates the initial temporal pulse broadening in the DC gun since this produces the greatest initial electron velocity distribution. In fact, for $\Delta E \approx$ 1eV, this effect alone introduces a pulse broadening of about 1ps for a 30kV DC photoelectron gun with a 1cm acceleration gap. After the DC gun, the longer time of flight down the UEM column allows the continual acceleration due to the pulse's internal space-charge field to affect the propagation dynamics.

In nearly all cases, the propagating pulse quickly develops a relatively linear velocity chirp which can be compensated for by an appropriately phased RF acceleration cavity in the UEM column [12,13]. The modeled UEM column therefore includes a RF cavity positioned 10cm after the DC photoelectron gun to study the conditions required to produce the shortest compressed electron pulse at the specimen. The RF cavity is chosen to be of the standard cylindrical design for oscillation on the fundamental TM_{010} mode at a frequency $\nu_{RF} = \Omega/(2\pi) = 1.4$GHz and to have a small ($<< \lambda_{RF}$) 1cm propagation length for the electrons through a small axial hole. The RF field experienced by the electron pulse can then be described by

$$E_{RF} = E_0 \sin(\Omega t + \phi) \ , \qquad (3)$$

where the phase ϕ of the RF field relative to the electron pulse in the cavity is set to preferentially accelerate the slower electrons at the back of the pulse. For a sufficiently strong RF field strength E_0, our analysis indicates that it is always possible to produce a short compressed pulse at the specimen a distance L = 10-100cm after the RF cavity – a result that is in agreement with prior analyses [14-16]. In other words, electron pulse broadening due to both longitudinal space-charge effects and the initial energy spread upon photoemission can be compensated for by the insertion of an RF cavity.

The model also revealed that another important and practical condition can also be met if the specimen is placed at a specific distance L behind the RF cavity: namely, that it is possible to arrange simultaneously for the electron pulse to have both the shortest pulse duration and the minimum energy spread at the specimen. An example of this condition is shown in Figure 11(b). For a DC gun voltage of 30kV over a 1cm gap, $\Delta E = \hbar\omega - \Phi$ = 1eV, and a space-charge field of 100V/m (corresponding to ~10^4 electrons/mm^2), a 1.4GHz RF cavity with a field strength of 6.85MV/m can simultaneously compresses the electron pulse to less than 20fs and reduce its energy spread to significantly less than 1eV at a distance L = 28.8cm. Clearly, this type of probe pulse for a DTEM could allow, for example, dynamic high-resolution electron energy loss spectroscopy (EELS) to be performed.

Unfortunately, operation of TM_{010} RF cavities of this type requires large RF power supplies. This is because machining tolerances on the internal copper walls of the cylindrical cavity restrict the cavity quality factor Q to ~1000. As a result, in order to provide the ~6.8MV/m field strength for the 1cm-long, 1.4GHz RF cavity described above, an RF power in excess if 100kW would be required. To a certain extent, this power requirement can be reduced through the use of higher RF frequencies [15] and re-

entrant RF cavity designs [16]. However, the required RF powers are still well outside the scope of this research project and, hence, probably outside the realm of a practical UEM.

Doubly-resonant and dielectric-loaded TM_{010} RF cavity

Current work on the design of an RF cavity for electron pulse compression is focusing on a dielectric-loaded $\lambda/2$-resonant TM_{010} cavity design. Such a cavity, in the form of a metal-coated dielectric cylinder with a 3-4mm-diameter hole down the axis for the electron beam, has some enormous potential advantages over the simpler, 'thin', and empty (evacuated) TM_{010} cavity described above. First, optical polishing techniques can be used to dramatically reduce the surface roughness, which will result in a significant enhancement of the Q of the RF cavity. Second, silver, a metal with a higher conductivity than copper, can be used to coat the dielectric, thereby further increasing Q. Third, electromagnetic boundary conditions dictate that the RF field strength experienced by the electron pulse inside the axial hole is ε_r, the relative permittivity, times larger than in the dielectric – a field enhancement. Fourth, each dimension of the RF cavity is reduced by a factor of about $\sqrt{\varepsilon_r}$ (i.e., by the refractive index at the RF frequency) when compared to the vacuum case, which reduces the volume and hence total energy stored in the cavity at resonance. All of these factors should contribute to a factor of 10^3 (or more) reduction in the required RF power for effective electron pulse compression in a UEM.

The use of a dielectric-loaded RF cavity has one further advantage over an empty cavity for use in a DTEM column where the electron velocities are generally around $c/2$ – corresponding roughly to a 100kV microscope. In an empty RF cavity, there is a mismatch between the phase velocity of the RF field (the speed of light c) and the group velocity of the electron pulse. This implies that there can be a significant 'slippage' of the optimum pulse compression condition over the electron pulse as it propagates through the RF cavity. In a dielectric-loaded RF cavity, this problem can be essentially removed by choosing a dielectric with the appropriate RF refractive index $\sqrt{\varepsilon_r}$ that allows the field phase velocity to be closely matched to the pulse group velocity. This velocity matching then also enables a $\lambda/2$-resonant TM_{010} cavity to be employed – a standard accelerator cavity in high-energy physics; that is, in our case, a RF cavity with a length $d = c/(2\nu_{RF}\sqrt{\varepsilon_r})$. The RF field experienced by the electron pulse in the 3-4mm-diameter hole can then be described by

$$E_{RF} = E_0 \sin\left(\frac{\pi z}{d}\right)\sin(\Omega t + \phi) , \qquad (4)$$

where z is the direction of propagation for the electron pulse. Two suitable dielectric (optical) materials that have low loss at GHz RF frequencies and have the appropriate refractive index have been identified: fused silica (SiO_2; $\varepsilon_r = 3.8$) and yttrium aluminum garnet (YAG; $\varepsilon_r = 10.4$).

Modeling of the performance of this novel dielectric-loaded TM_{010} RF cavity is now underway. Figure 12 shows some preliminary data for a 3GHz YAG-loaded cavity for an

incident electron pulse with a velocity of $c/3 = 10^8$m/s and linear negative velocity chirp (faster electrons at the leading edge of the pulse). The fully relativistic model indicates that for different RF phases ϕ between zero and π there exists a field strength that reverses the velocity chirp (Figure 8(a)). The optimum value of ϕ giving the minimal required RF field strength of about 1MV/m for this pulse compression condition is about $\pi/2$. Figure 8(b) shows the reversal in the velocity chirp for the electron pulse under this optimal condition as it propagates through the 16mm RF cavity length. Similar results are obtained for fused silica.

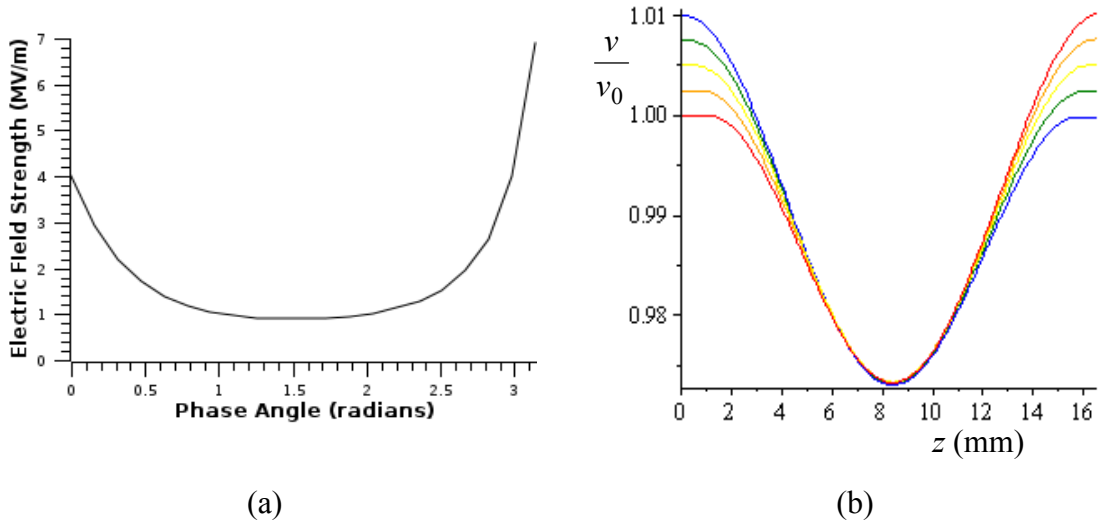

(a) (b)

Figure 12. Conditions for electron pulse velocity chirp reversal in a $\lambda/2$ TM_{010} RF cavity loaded with the dielectric YAG (yttrium aluminum garnet) when the incident pulse velocity $v_0 = c/3$: (a) Required RF electric field amplitude E_0 as a function of the phase angle ϕ; (b) Reversal of the velocity chirp for five normalized electron velocities in the pulse upon propagation through the 16mm RF cavity length when $\phi = \pi/2$ and $E_0 = 1$MV/m.

Armed with knowledge of the required RF field strength for velocity chirp reversal, an estimate may be made for the RF power that needs to be supplied to 3GHz cavity. For the above case, a YAG-loaded cavity operating with $E_0 = 1$MV/m, a conservative estimate using $Q = 1000$ indicates that less than 10W of RF power would be required. This is well within the capabilities of modern semiconductor-based RF amplifiers. Consequently, efforts are now underway to find a vendor to provide the custom polished optic and the electronics required to synchronize the resonant TM_{010} RF cavity frequency to a harmonic of the 63MHz femtosecond Yb:KGW laser employed to drive the photocathode.

The work performed at ASU aims to develop a fully coherent monochromatic photofield electron source, driven by a pulsed laser. Field-emission sources are the brightest particle sources in all of Physics, and the photofield effect may allow this coherence and brightness to be combined with the speed of fast pulsed lasers. (Recent

work has demonstrated sub-femtosecond field emission pulses - see PRL 97, 247402 (2006)). Over the past year we have (i) Found the optimum procedure for GaAs photofield tip preparation using a sequence of wafer cleavage, chemical etching, FIB shaping, chemical etching and controlled heating in UHV. (ii) This process produces photoactive surfaces on intrinsic GaAs field-emission needles, for which we have demonstrated a thousand-fold increase in electron current under illumination. Fowler-Nordheim curves and quantum efficiencies have been measured. (iii) Point-projection "shadow" images and Fresnel biprism fringes have been obtained in our small chamber, which is fitted with a tip exchange mechanism and 120 C bake capability. The chamber also provides field-emission microscope images of the tips. Because the lensless point-projection imaging mode avoids coulomb interactions at beam cross-overs, we expect it to be capable of very high speed, however penetration is limited. Fast imaging experiments will be conducted using molecules within carbon nanotubes as the sample. The resolution in this mode is about equal to the electron source diameter of 1 - 2nm. By chopping the laser beam, we aim to measure the pulse duration on this mode. (iii) A second chamber (bakeable to 200C) has been constructed and fitted with tip heating facilities, thermocouple, and CHA energy spectrometer. This spectometer is being used to measure the energy spread in the beam as a function of the laser energy, since there is much interest also in highly monochromatic electron beams. (In the simplest model, the electron beam energy is about equal to the difference between the laser energy and the GaAs bandgap). Early in 2008 we obtained electron energy spectra due to photofield emission from GaAs needles driven by lasers of three different energies. (These are the first observations ever of the energy distribution in photofield emitters). Physics graduate student Vecchione expects to finish his PhD on this project in 2008. Two companies (FEI and Nion) have shown interest in this photofield electron source for applications in electron microscopy and energy-loss spectroscopy.

---

1. "Low-threshold, dual-passive mode locking of a high-power, thermal-lens-shaped Nd:$GdVO_4$ laser," S.L. Schieffer, D. Brajkovic, A.I. Cornea, and W.A. Schroeder, Optics Express **14** (2006) 6694-6704.
2. "High-power, femtosecond, thermal-lens-shaped Yb:KGW laser," J.A. Berger, M,J. Greco, and W.A. Schroeder, paper CMS6, Conference on Lasers and Electro-Optics 2008 (CLEO'08), May 4-9, San Jose, California.
3. "High-power, femtosecond, thermal-lens-shaped Yb:KGW oscillator," J.A. Berger, M,J. Greco, and W.A. Schroeder, submitted to Optics Express (March 2008).
4. N.W. Rimington, S.L. Schieffer, W.A. Schroeder, and B.K. Brickeen, "Thermal lens shaping in Brewster gain media: A high-power, diode-pumped Nd:$GdVO_4$ laser," Optics Express **12**, 1426-1436 (2004).
5. "Mode-locked Yb:KGW laser longitudinally pumped by polarization-coupled diode bars," G.R. Holton, Optics Letts. **31** (2006) 2719-2721.
6. "CeB_6 electron gun for low-emittance injector," K. Togawa, T. Shintake, T. Inagaki, K. Onoe, and T. Tanaka, Phys. Rev. Special Topics – Accelerators and Beams **10** (2007) 020703.
7. "Field emission as a tip nanometer source of free electron femtosecond pulses," P. Hommelhoff, Y. Sortais, A. Aghajani-Talesh, and M.A. Kasevich, Phys.Rev.Lett. **96** (2006) 077401.
8. "Ultrafast electron pulses from a tungsten tip triggered by low-power femtosecond laser pulses," P. Hommelhoff, C. Kealhofer, and M.A. Kasevich, Phys. Rev. Lett. **97** (2006) 247420.
9. "Evanescent-wave acceleration of ultrashort electron pulses," J. Zawadzka, D.A. Jaroszynski, J.J. Carey, and K. Wynne, Appl. Phys. Lett. **79** (2001) 2130-2132.

10. "Ponderomotive acceleration of photoelectrons in surface-plasmon-assisted multiphoton photoelectric emission," J. Kupersztych, P. Monchicourt, and M. Raynaud, Phys. Rev. Lett. **86** (2001) 5180-5183.
11. "Anomalous multiphoton photoelectric effect in ultrashort time scales," J. Kupersztych and M. Raynaud, Phys. Rev. Lett. **95** (2005) 147401.
12. "Ultrafast electron optics: Propagation dynamics of femtosecond electron packets," B.J. Siwick, J.R. Dwyer, R.E. Jordan, and R.J.D. Miller, J. Appl. Phys. **92** (2002) 1643-1648.
13. "Femtosecond electron pulse propagation for ultrafast electron diffraction," B.W. Reed, J. Appl. Phys. **100** (2006) 034916.
14. "Sub-fs electron pulses for ultrafast electron diffraction," E. Fill, L. Veisz, A. Apolonski, and F. Krausz, New Journal of Physics **8** (2006) 272.
15. "Hybrid dc-ac electron gun for fs-electron pulse generation," L. Veisz, G. Kurkin, K. Chernov, V. Tarnetsky, A. Apolonski, F. Krausz, and E. Fill, New Journal of Physics **9** (2007) 451.
16. "Electron source concept for single-shot sub-100 fs electron diffraction in the 100keV range," T. van Oudheusden, E.F. de Jong, S.B. van der Geer, W.P.E.M. Op 't Root, O.J. Luiten, and B. J. Siwick, J. Appl. Phys. **102** (2007) 093501.

2. A comparison of accomplishments with the original goals and objectives

It was originally proposed that the DTEM be used to study the dynamics of metallic and semiconducting nanomaterials. All CDI algorithms apply what is known as a support constraint to the real space image of the diffracting object. This constraint sets image intensities outside of a specified area known as the support to zero. Originally this meant a priori information about the shape of the object was required to perform CDI, however recent developments in the field allow for algorithms that compute the support area as the iterations progress. Since the camera length at which a diffraction pattern is recorded will determine the largest resolution attainable in a reconstructed image, electron microscopes (with their limited range of camera lengths) are only suitable for CDI experiments involving nanoscale objects. This makes CDI an ideal technique for enhancing the performance of the DTEM for experiments involving nanomaterials. Thus far the DTEM has been successfully used to demonstrate the feasibility of this technique. As the coherence and brightness of the electron source in the microscope continues to improve with future upgrades, the value of utilizing CDI in the DTEM will only grow. As a technique that is uniquely suited to nanoscale objects it should fit in very well with the stated objective of imaging the growth and dynamics of a wide variety of nanomaterials. The development of the in-situ stage also allows nanostructures to be studied in detail over a wide range of ambient conditions. Coupled with the advancements in CDI that have been developed, the stage is set for significant experiments to be performed in year 3.

The research accomplishments at UIC over the last 21½ months (since the fiscal initiation of the sub-contract in May 2006) are compared below with the original goals and objectives that are bulleted and in *italics*.

- *Construct the versatile ultrafast electron microscope (UEM) test column, and interface the column with both the available, state-of-the-art, diode-pumped, ultrashort-pulse laser system and parts from a decommissioned JEM 100CX electron microscope (the magnetic electron lens, scintillator, and sample holder stage).*

A test-bed photo-electron gun has been successfully constructed and its photocathode is now driven by an upgraded laser system – a soliton mode-locked Yb:KGW laser delivering 200-300fs pulses (see Section 1 above). However, the late installation of the custom optical table in the dedicated laboratory for the UEM in September 2007 has delayed the interfacing of our photoelectron gun to the JEM 100CX column.

- *Characterize the functionality of the UEM test column using simple, planar, laser-driven photocathodes (e.g., Ta, LaB_6, Ag, Au, etc.).*

Several large-area, planar photocathodes have been investigated in detail. The hexaborides LaB_6 and CeB_6 are now being studied in a re-designed DC photoelectron gun using powerful second harmonic (520nm) femtosecond pulses from the new Yb:KGW laser (see Section 1 above).

- *Design the RF electron pulse compression cavity and associated reactance-balanced and resonant LCR circuit.*

The design of the RF electron pulse compression cavity has undergone significant changes in order to allow its implementation to fall within the realm of this research project (see Section 1 above). The performance of the new design, a dielectric-loaded TM_{010} RF cavity, is currently being assessed and is expected to be specified for manufacture by May 2008.

- *Conduct initial tests on Si nano-patterned photocathodes produced using ultra-violet laser interference lithography.*

The initial tests on Silicon nano-patterned photocathodes employing gold nano-particle arrays have been delayed due to unforeseen problems in manufacture by soft lithography at the Northern California Nanotechnology Center (NC2), the nano-fabrication facility at our collaborating institution UC-Davis. Initial nano-patterned photocathode test samples are expected to be available in May 2008. A complementary method to test the idea of coherent plasmon-enhanced photoemission using a plane holographic gold grating is now currently being pursued.

- *Coordinate research efforts with collaborators from UC-Davis, ASU, and LLNL.*

There has been frequent contact between co-PI Schroeder, Co-PI Spence, and PI Browning on various aspects of the research program. Schroeder and Spence visited LLNL in June 2006 to discuss the coordination of the research program's efforts and its potential impact and benefit to the active DTEM project at LLNL. The exchange of ideas with the scientists working on the LLNL DTEM project has proved useful to the effort at UIC. The NNSA 2007 Stewardship Science Academic Alliances (SSAA) Program Symposium, in Washington, DC, on February 5-7, 2007, provided an additional opportunity for PI Browning and co-PI Schroeder to continue their coordination discussions,

A further similar opportunity was provided by the NNSA 2008

Stewardship Science Academic Alliances (SSAA) Program Symposium, in Washington, DC, on February 26-28, 2008, where it was decided to send Joel Berger to LLNL in June or July 2008 to work on the operational DTEM at LLNL. A prior visit to LLNL in early May 2008 is also being arranged.

- *Design and have fabricated custom nano-patterned photocathodes for improvement of the initial spatial coherence of electron pulses generated by a laser-driven (linear or nonlinear optical) photoemission processes.*

Fabrication of the array of gold nano-disks on silicon originally proposed to improve the spatial coherence of electron pulses (i.e., lower the photocathode emittance) is proving problematic. As a result, plasmon-enhanced nano-patterned photo-emitters based on plane holographic gold gratings are now being evaluated. A commercial source for a 'criss-cross' holographic grating serving as a plasmon-enhanced array of nano-emitters has also been found.

- *Investigate the spatial coherence of electron pulses generated by patterned photocathodes after propagation down the UEM test column (i.e., study the space-charge effects).*

This goal is dependent upon the availability of the nano-patterned photocathodes. Consequently, this investigation has only just been initiated using plane holographic gold gratings, where efficient resonantly-excited plasmon-enhanced photoemission is expected.

- *Incorporate and characterize the performance of the RF electron pulse compression cavity.*

As a suitable design for a RF compression cavity was not found until late in Year 2 of the project this project goal will be met in Year 3. However, the design phase is now nearly complete and a vendor capable of manufacturing the novel dielectric-loaded TM_{010} RF cavity to the desired specifications has been found.

For the ASU component of this research, we originally we had two goals. One was to make a monochromatic electron field emitter, and the second to make a fast, laser-pulsed field emitter. Our accomplishments to date are well aligned with the original goals for the whole project. The pulsed emitter is working , showing a thousand-fold enhancement of field emission current under laser illumination, and the second vacuum chamber is complete and operating, fitted with an energy spectrometer. Very recently we have obtained our first spectra showing the energy spread in the beam. A new idea, which arose over the last year, has been to use the point-projection shadow image mode (whose resolution is about 2nm) to obtain femtosecond images , taking advantage of the fact that the lensless diverging beam is not limited in speed by Coulomb interactions.

4. Schedule status

Below is a list of key milestones (bulleted and in *italics*) and their status for the UC-Davis portion of the three-year research project:

Year 1: 03/01/06 – 02/28/07

- *Identify and hire two exceptional graduate students to perform the work in this proposal.*

  One graduate student has been hired in the first year of this project (Daniel Masiel). There are several students and post-docs working part-time on the project (Judy Kim, Marta Bonds, Mitra Taheri) that either are just starting (supported by the department) or are supported from other funds. The second student will be hired in the summer this year after the first year of coursework is completed.

- *Perform initial tests of in-situ specimen stage on conventional TEM at UC-Davis*
- *Design and order optimized in-situ stage for the DTEM (stage to be property of UC-Davis)*

These tests have been performed and a final design for the DTEM stage has been delivered to Fischione. This stage will be delivered in September 2007.

- *Evaluate existing spectrometer at LLNL for use in the second and third year experiments. Design spectroscopic experiments to be carried out in year 2 and 3.*

LLNL has no current plans to move a spectrometer onto the DTEM. The cost of the spectrometer included in the original proposal was not included in the final budget. This aspect of the proposed work is on hold until the spectrometer becomes part of the operational plan again.

- *Perform initial experiments on structural phase transformations focusing on optimization of electron beam intensity and control of the pump laser energy (aiming for precise control of transformations).*

Initial experiments on phase transformations have been performed at LLNL. Amorphous to crystalline phase transformations, martensitic transformations and nanostructure growth have been found to be controllable in the DTEM. The CDI development described earlier in the report is designed to optimize the ability to observe these transformations in nanostructures.

- *Perform first experiments on grain boundary de-faceting.*

Experiments have been designed in collaboration with Sandia National Laboratory. Initial experiments have been delayed pending a new postdoc who will provide samples.

Year 2: 03/01/07 – 02/29/08

- *Identify and hire two exceptional graduate students to perform the work in this proposal.*

A second graduate student, Jeffery Aguiar, has now been hired to work on this research.

- *Utilize the in-situ stage for analysis of nanoscale materials systems.*

The in-situ stage design has now been completed and the first experiments performed. Work in year 3 will continue to use this stage for the de-facetting and phase transition experiments.

Below is a list of key milestones (bulleted and in *italics*) and their status for the UIC portion of the three-year research project:

Year 1: 03/01/06 – 02/28/07

- *Construct the versatile ultrafast electron microscope (UEM) test column, and interface the column with both the available, state-of-the-art, diode-pumped, ultrashort-pulse laser system and parts from a decommissioned JEM 100CX electron microscope (the magnetic electron lens, scintillator, and sample holder stage).*

  The late installation of the custom optical table in the dedicated laboratory for the UEM in September 2007 has delayed the interfacing of our photoelectron gun to the JEM 100CX column: a test-bed picosecond laser-driven photo-electron gun has been in operation since August 2006 and was upgraded with a femtosecond drive laser source in October 2007.

- *Characterize the functionality of the UEM test column using simple, planar, laser-driven photocathodes (e.g., Ta, LaB_6, Ag, Au, etc.).*

  On schedule and in progress: several planar photocathode materials have been studied in a test-bed picosecond laser-driven photo-electron gun and a promising set of new photoemitters based on plasmon-enhanced photoemission are being studied. Theoretical studies of electron pulse propagation and focusing have laid the operational framework of the UEM test column.

- *Design the RF electron pulse compression cavity and associated reactance-balanced and resonant LCR circuit.*

  Behind schedule: a suitable design for a RF compression cavity driven by a low-power RF supply was not found until late in Year 2. The new RF cavity design requires a different coupling to the RF source – inductive coupling.

- *Conduct initial tests on Si nano-patterned photocathodes.*

  Approximately 15 months behind schedule due to problems in manufacture: studies expected to start in Spring 2008.

- *Coordinate research efforts with collaborators from UC-Davis, ASU, and LLNL.*

  On schedule.

<u>*Year 2: 03/01/07 – 02/29/08*</u>

- *Design and have fabricated custom nano-patterned photocathodes for improvement of the initial spatial coherence of electron pulses generated by a laser-driven (linear or nonlinear optical) photoemission processes.*

  Plasmon-enhanced nano-patterned photo-emitters based on plane holographic gold gratings are being evaluated. A commercial source for a 'criss-cross' holographic grating serving as a plasmon-enhanced array of nano-emitters has been found. The manufacture of Si substrate nano-patterned photocathodes (an array of isolated gold nano-disks) is proving problematic (roughly 15 months behind schedule).

- *Investigate the spatial coherence of electron pulses generated by patterned photocathodes after propagation down the UEM test column (i.e., study the space-charge effects).*

  Simple (and intuitive) tests have been proposed to measure the degree of spatial coherence and/or emittance of electron pulses generated by patterned photocathodes. Experimental studies are in progress.

- *Incorporate and characterize the performance of the RF electron pulse compression cavity.*

  Behind schedule: a suitable design for a RF compression cavity, which did not require a large RF power supply, was not found until late in Year 2 of the project. The design phase is now nearly complete and a vendor capable of manufacturing the dielectric-loaded TM_{010} RF cavity to the desired specifications has been found.

Year 3: 03/01/08 – 02/28/09

- *Find conditions (e.g., number of electrons in pulse, photocathode nano-pattern structure, RF cavity parameters, etc.) that optimize the spatio-temporal coherence of electron pulses at the sample and determine the resulting space-time resolving power of the test UEM.*

  Ahead of schedule: modeling of a canonical pulsed electron source has defined the basic conditions required to temporally compress the electron pulse in order to generate the shortest pulse at the specimen.

- *Incorporate the laser-driven, field-emission, fiber-tip source into the UEM test column and compare its performance to that of the large-area, nano-patterned photocathodes.*

5. Any changes in approach and why

In Years 1 & 2, there have been no major changes in the scientific approach to the work conducted at UC-Davis.

In Years 1 and 2 of the research project period, there have been no significant changes in the basic scientific approach for the work conducted at UIC. However, some research findings have necessitated some changes in the methods employed. These are outlined below:

- The procurement of the nano-patterned materials required to test the idea of generating a high spatial coherence electron pulse from a large-area photocathode by using a phased array of laser-driven field emitters has proven problematic. Laser interference lithography cannot produce such photo-emitter arrays with the necessary precision and dimensional tolerance, and the alternative soft lithography technology (available at the Northern California Nanotechnology Center (NC2) at our collaborating institution UC-Davis) is proving challenging.

Consequently, a complementary method to test the idea of coherent plasmon-enhanced photoemission using a plane holographic gold grating is now also being pursued.

- The finding that ~10ps pulses from a Nd:$GdVO_4$ laser may not be short enough to allow the study of the emittance and potential coherence of nano-patterned photocathodes has resulted in the use of a more suitable diode-pumped Yb:KGW laser, which generates pulses with a duration of 200-300fs.
- The recognition that the initially proposed RF cavity design would require a prohibitively large RF power supply initiated an extensive study of other similar approaches. This has resulted in a novel concept for the compression of ultrashort electron pulses in a UEM – a dielectric-loaded TM_{010} RF cavity. Numerical analysis of this cavity suggest that its performance is superior and that its can operate with a substantially reduced RF power supply.

One further item is noteworthy. In the September 2007, the ultrafast electron microscopy project at UIC was moved into dedicated laboratory space in the Research Resources Center – East. This move will benefit the UIC portion of the research work on the photo-electron gun design and the DTEM test column construction and characterization by (i) improving the environmental laboratory conditions (vibration, temperature control, etc.), (ii) placing the project in a more secure restricted access area, while (iii) allowing future access to the instrument for all scientists under the auspices of the UIC Research Resources Center.

In Years 1 and 2 of this three-year project period, there have been no changes in the approach to the research project at ASU.

6. Actual or anticipated delays and actions taken

In Years 1 and 2 of this three-year project period, there have been a few minor delays in the progress of the work on the research project at UC-Davis:

(i) There have been minor delays in obtaining samples from the collaborators. Work has moved forward in the development of the methods and the in-situ stage to be ready for the samples when they become available.

(ii) The second graduate student was not hired immediately in year 1. Graduate students still working on the coursework were used to supplement the work done on the project. Given the change in the design of the photocathodes at UIC, the student support was used for the nanopatterned lithography. The second graduate student, Jeffery Aguiar, has now been hired.

In Years 1 and 2 of the three-year project period, there have been a few delays in the progress of the work on the research project at UIC:

(i) The sub-contract negotiations between UC-Davis and UIC delayed all financial actions on the UIC portion of the project until mid-May 2006. No action by co-PI Schroeder was possible on this issue.

(ii) The delay in the acquisition of the custom optical table required for the construction of the versatile ultrafast electron microscope test column has not caused significant problems. The photoelectron gun developed in the first few months of Year 1, together with the available picosecond Nd:$GdVO_4$ laser, have proved adequate for much of the initial research work.

(iii) The realization that laser interference lithography was probably not the best method to fabricate the nano-patterned photocathodes has not caused a major delay since an alternative fabrication technique – soft lithography at UC-Davis – was quickly found. Unfortunately, the new nano-fabrication technique has proven difficult to implement, causing a delay in this aspect of the project. However, an alternative and parallel method to study plasmon-enhanced photoemission using plane holographic gold gratings in now underway.

(iv) The recognition that the originally planned RF cavity would require a power supply outside the scope of the research project led to a significant amount of work to find a solution to the problem. The innovative solution – a dielectric loaded TM_{010} RF cavity – was found towards the end on Year 2 and is now in the final design stage prior to manufacture.

(v) At the end of Year 1, it was also recognized that the picosecond Nd:$GdVO_4$ laser was not a suitable laser source for the project. Consequently, at the same time that the project was moved into a dedicated UEM laboratory in September 2007, a new femtosecond Yb:KGW laser radiation source was commissioned for the project.

In Years 1 and 2 of this three-year project period, there have been a few minor delays in the progress of the work on the research project at ASU that have not resulted in any significant change to the work plan.

7. Changes in key personnel

There are no changes in key personnel. So far, 4 graduate students have been identified to work on this project: Daniel Masiel (UCD), Jeffery Aguiar (UCD), Joel Berger (UIC) and Theo Vecchione (ASU).

8. Tech transfer activities

Below are listed the publications and presentations that resulted from the work on the research project after March 2006. Included are known future publications, submissions, or presentations.

Research articles:

1. “High-power, femtosecond, thermal-lens-shaped Yb:KGW oscillator,” J.A. Berger, M. J. Greco, and W.A. Schroeder, submitted to Optics Express (March 2008).

Presentations:

14. **Invited:** “Optimization of ultrafast photo-electron sources for DTEM,” W.A. Schroeder, Microscopy and Microanalysis (M&M 2008), August 3-7, 2008, Albuquerque, New Mexico.

13. **Contributed:** “High-power, femtosecond, thermal-lens-shaped Yb:KGW laser,” J.A. Berger, M,J. Greco, and W.A. Schroeder, paper CMS6, Conference on Lasers and Electro-Optics 2008 (CLEO’08), May 4-9, San Jose, California.

12. **Invited:** “Combining Spatial and Temporal Resolution in the Dynamic TEM,” N. D. Browning, J.A. Berger, G.H. Campbell, J.S. Kim, W.E. King, T.B. LaGrange, D.J. Masiel, B.W. Reed, W.A. Schroeder, J.C.H. Spence, M.L. Taheri, and T. Veccionne, Microscopy and Microanalysis (M&M 2007), August 2007, Fort Lauderdale, Florida.

11. **Contributed:** "Monochromatic Photo-Field Electron Emission Sources," T. Vecchione, G. Hembree, U. Weierstall, J. Spence, and N. Browning, American Physical Society 2007 March Meeting (APS March 2007), March 2007, Denver, Colorado.

10. **Invited:** “Enhanced Functionality for Materials Analysis in the Dynamic TEM (DTEM),” N. D. Browning, D.J. Masiel, M.L. Taheri, J.A. Berger, W.A. Schroeder, T. Vecchione, and J.C.H. Spence, NNSA 2007 Stewardship Science Academic Alliances (SSAA) Program Symposium, February 5-7, 2007, Washington, D.C..

9. **Contributed:** "Laser-Driven GaAs Field-Emitter," T. Vecchione, U. Weierstall, G. Hembree, and J. Spence, NNSA 2007 Stewardship Science Academic Alliances (SSAA) Program Symposium, February 5-7, 2007, Washington, D.C..

8. **Contributed:** “Enhanced Functionality for Materials Analysis in the Dynamic TEM (DTEM): Space-Time Electron Pulse Propagation Dynamics,” J.A. Berger, N.D. Browning, and W.A. Schroeder, NNSA 2007 Stewardship Science Academic Alliances (SSAA) Program Symposium, February 5-7, 2007, Washington, D.C..

7. **Invited:** “Advances in TEM for Materials Science”, Nigel D. Browning, November 6th, 2006, IBM-Almaden.

6. **Contributed:** "Monochromatic Photo-Field Electron Emission Sources," T. Vecchione, U. Weierstall, C. Edgcombe, and J. Spence, The 16th International Microscopy Congress (ICEM 2006), September 2006, Sapporo, Japan.

5. **Invited:** “Dynamic TEM”, N. D. Browning, M. R. Armstrong, G.H. Campbell, J. S. Kim, W. E. King, T. B. LaGrange, C. J. Mitterbauer, and B. W. Reed, Workshop on 2-D Crystallography, University of California, Davis, Ca, August 6-10, 2006

4. **Invited:** “The Potential of Single Shot Dynamic TEM for Combined Nanosecond and Nanoscale In-Situ Microscopy”, N. D. Browning, M. R. Armstrong, G.H. Campbell, J. S. Kim, W. E. King, T. B. LaGrange, C. J. Mitterbauer, and B. W. Reed, 64th Annual Meeting of the Microscopical Society of America, Chicago, IL, July 30-August 3, 2006.

3. **Contributed:** “Space-Time Propagation Dynamics of Gaussian Electron Pulses,” J.A. Berger and W.A. Schroeder, Late Breaking Poster LB-31, Microscopy and Microanalysis (M&M 2006), July 30 – August 3, 2006, Chicago, Illinois

2. **Contributed:** "Monchromatic Photo-Field Electron Emission Sources," T. Vecchione, U. Weierstall, C. Edgcombe, and J. Spence, Microscopy & Microanalysis (M&M 2006), July 30 – August 3, 2006, Chicago, Illinois

1. **Invited:** “Ultrafast Electron Mircoscopy: The Problem of Spatial Coherence,” W.A. Schroeder, Microscopy and Microanalysis (M&M 2006), July 30 – August 3, 2006, Chicago, Illinois.

Collaborations:

An unforeseen collaboration, between UC-Davis and photocathode design effort at UIC, is being initiated for the fabrication of nano-patterned photocathodes using the Northern California Nanotechnology Center at UC-Davis.